

# A Local/Global Space for Contour Partitioning and Description

C. Rasche

Abteilung für Allgemeine Psychologie  
Justus-Liebig Universität  
Otto-Behagel-Str 10, F1  
D-35394 Giessen, Germany

+ 49 (0) 641 99 26 133 (phone)

+ 49 (0) 641 99 26 119 (fax)

rasche15@gmail.com

[www.allpsych.uni-giessen.de/rasche](http://www.allpsych.uni-giessen.de/rasche)

## **Abstract**

A contour decomposition is proposed that allows partitioning and parameterizing contours. The decomposition firstly transforms the contour geometry into a local/global space by an iteration process that labels a selected segment and measures its amplitude. This space enables determining the location of high-curvature points, which however is a scale and context-dependent issue. From the local/global space an abstraction can be formed, from which geometric parameters such as curvature, smoothness, symmetry and edginess are derived. The decomposition output can explain a number of visual pop-out variances just by taking the difference across parameter values.

## **Keywords**

contour geometry, contour partitioning, segment labeling, shape description, parallel pop-out

## **Introduction**

When we see a structure such as a shape or object, we can determine its points of highest curvature and label the contour segments in between by a geometric attribute such as straight, curved or wiggly (Attneave 1954; Fischler and Bolles 1983). One can assume that at those points a shape is partitioned and that the resulting segments are assigned an attribute such as. The prevailing principle to arrive at such a description is the integration of local orientations, which was suggested by Hubel and Wiesel already (Hubel and Wiesel 1968). The principle has been applied in many neural network simulations, e.g. (Riesenhuber and Poggio 1999; VanRullen and Thorpe 2002; Hansen and Neumann 2004), and it has also been proposed as a psychophysical model (Feldman 2001). This integration essentially corresponds to template matching as the contour is not transformed: merely the relative spatial locations of the local orientations are stored. However, template matching is potentially cumbersome when manipulating with

structure; for instance when replicating a figure by drawing, e.g. (Coen-Cagli, Coraggio et al. 2009), template memorization is a brute-force solution. An alternative principle could be that a decomposition of the contour segment takes place, whose output describes the contour geometry by a few parameters. In such a scenario, only the parameter values had to be remembered during the copying process. Analogously, if shapes were represented by contour parameters, then this could provide a solution to the issue of structural variability, the fact that different shape instances are often slightly different in their exact spatial relations and contour geometries. This variability appears as subtle and that is the reason why it is tempting to think that low-pass filtering can absorb this variability. This is implicitly assumed in neural network approaches when they generate a pyramidal scale space (fine/coarse axis). But low-pass filtering includes a loss of information and can therefore not lead to a precise localization of high-curvature points (Fischler and Bolles 1983); nor can it lead to an accurate shape description. Instead, it is indispensable to analyze the structure without modifying it, specifically by making systematic distance measurements with increasing window size. We call this the *local/global* space, or LG space. In this space it is facile to localize high-curvature points by a maximum operation and it allows deriving parameters that describe the geometry of the partitioned segments. We will show that if one uses those parameters as vectors, that category-typical contours can be determined.

## ***Model***

### **Overview**

Contours appear with a large variety of geometric characteristics: a contour can be wiggly or irregular, a characteristic of many natural contours; a contour can be straight as in tree stems; a contour can be undulating, a characteristic that occurs in animal silhouettes (snake; neck and back of many animals); or a contour can be geometrically precise outlining for instance a particular landscape horizon. Describing and identifying contours in this way requires a method which explicitly captures these characteristics. The method presented here assumes that the elements of contour description are straight and curved segments, and that any contour can be regarded as an alternating sequence of those elements. For a natural contour, this sequence is typically irregular, for an oscillating contour the sequence is even. In the special case of an arc or straight line, there is no sequence but just one element. To identify these geometric elements, it requires the corresponding filter mechanisms. A contour is therefore iterated with a function that labels the segment as straight or curved and that measures the segment's amplitude. For a given window size, this iteration process generates a signature, which already allows to characterize curvatures in great detail. As the contour size is not known

a priori, these signatures are created for a range of window sizes resulting in the LG space.

In this study we introduce an algorithmic solution to this description, but we will also loosely sketch a neural network solution in the discussion section.

### Generating Signatures

The methodology is introduced with the label selecting curved segments, or hereafter also called bows (figure 1). The contour, with arc length variable  $v$ , is iterated with a window (a chord or stick) of fixed length  $\omega$ . If such a selected subsegment lies primarily on one side of the straight line  $l$  connecting its endpoints, then the subsegment is labeled a bow and the subsegment's amplitude  $a_{max}$  is assigned to a 'bowness' signature,  $\beta_{\omega}(v)$ , otherwise the value is set to 0. Figure 1a to f shows the signature for different geometries, such as smooth arc, L feature, round corner (smooth arc with straight segments at the ends), flat bow, sharp bow and asymmetric bow. The advantage of this signature is that it is a one-dimensional signal, which can be easily analyzed to derive some geometric characteristics. We now call the range of neighboring signature values which are greater 0, a *bowness-function block*  $\beta^{\square}$  (or 'function block' or just 'block'). Its degree of *circularity*  $\zeta^{\square}$  is given by its integral:  $\zeta^{\square} = \int \beta^{\square}$ . The location of the maximum's amplitude corresponds to the point of highest curvature. The block's overall evenness expresses the symmetry  $v^{\square}$  of the segment.

[Figure 1]

To distinguish whether the block represents an L feature or an arc (figure 1a versus 1b) two steps are performed. First, the derivate of  $\beta^{\square}$  is determined. In case of an L feature the derivative is decreasing, in case of a smooth arc it is a constant function with value equal 0 and in case of a flat bow (figure 1d) it is increasing. In a second step, the derivative is multiplied by a normalized, ramp function  $F^f$ , - essentially the derivative for an L feature -, whose width is equal to the block size (with center value equal 0). The integral of this multiplication defines the parameter *edginess*  $\varepsilon^{\square}$  (in summary:  $\varepsilon^{\square} = \int \beta^{\square}(v) F^f(v)$ ). The edginess value is hence positive for an L feature, null for a perfect arc and negative for a flat bow.

### Local/Global Space

The signatures in figure 1 are made with a window size of optimal size. But as contours show arbitrary geometry, these signatures are determined for a range of window sizes leading so to the LG space. This space is sketched in figure 2 for a contour whose global shape describes a single inflexion. At a local scale (scale meaning here window size), the

contour consists of two smooth arcs, whose high-curvature points are marked by p1 and p3; the bowness signature therefore shows two function blocks (figure 2b, p1 and p3; it is emphasized that this is a schematic and the function blocks do not match exactly the functions shown in figure 1). To detect the change of sign at point p2, we introduce a second label, the inflexion label (transition; change of sign). It selects contour segments whose points lie on both sides of the straight line  $l$ , leading thus to the inflexion signature  $\tau(v)$ , shown in gray in figure 2b. Because there is only one such change at a local level, the inflexion signature shows only one function block. At a global scale, only the inflexion signature shows a function block as the global geometry of the contour describes an inflexion. The local/global space is sometimes abbreviated  $\beta_{\omega}(v)$  or  $\tau_{\omega}(v)$ .

[Figure 2]

Deriving the contour geometry from this LG space is now a bit more complicated – than in the case of the previously introduced signatures, but the algebraic operations outlined above still hold in principle. But before moving on to a global description, we firstly address the issues of selecting high-curvature points and contour partitioning. This is better illustrated on an implementation of the LG space, see figure 3. The smallest window sizes were  $\omega = [5, 7, 9, 11, 15]$  (number of contour pixels), larger window sizes were generated in increments of  $\sqrt{2}$ . The amplitudes of the signatures were normalized by the window size.

At a local scale, the size and location of the function blocks occur irregular due to the uneven layout of the contour at that scale - and partly due to the aliasing problem. At a global scale, the function blocks are more even and regular.

A third label is now introduced, the straightness label, which is necessary, because the lack of a bowness or inflexion block is not unique enough to determine whether a segment is straight or not  $\gamma(v)$ . Complete straightness is indicated by an amplitude set to a value of 0.5 (straightness label stippled in figures 3-6), whereas a value of 0 means lack of straightness. The straightness signature is suppressed (set to 0) at those locations, where a (positive) bowness signature value at the same location is present, either in the same window or at any more global level.

[Figure 3]

**High-curvature point selection:** The selection of high-curvature points is now a scale-dependent issue. If the goal is to describe the contour loosely only, then a selection at a global window suffices for which two high-curvature points can be localized (e.g. window no. 6, amplitude maximum at pixels no. 23 and 53). If the contour is to be

described accurately, then a selection of a local window is necessary for which three or four curvature points are selected (e.g. window no. 3, maximum at pixels no. 9, 22 and 49; small function blocks ignored). Thus, the number and precise location of the high-curvature points (and hence arcs) varies with scale selection.

An analogous scale selection has to be made, when one intends to copy a figure by drawing, because a decision has to be made on the desired degree of copying fidelity (Coen-Cagli, Coraggio et al. 2009). For a low fidelity, a global scale will suffice and only a few fixations with large spacing along the contour are made, which was probably the strategy for observer 2, 5, 6 and 8 (figure 7 in (Coen-Cagli, Coraggio et al. 2009)); for a high fidelity, fixations at a more local scale are necessary and hence many saccades are made with a small spacing between fixations (see observers 3, 4, 9 and 10 in figure 7 in (Coen-Cagli, Coraggio et al. 2009)). Due to the diversity of the observer's scan paths, it is not clear whether there exist strategies with regard to the exact fixation location on the contour, e.g. whether observers fixated high-curvature points or points of lowest curvature. Any such fixation precision is also difficult to determine, as the eye-tracker measurement error is at least 0.5 degrees in general (e.g. (Tatler, Baddeley et al. 2005)) or due to the possible inaccuracy in visual orientation (Rasche and Gegenfurtner 2010). But the crucial point here is that the LG space provides a rich geometric description that allows a quick abstraction depending on the desired description accuracy.

## **Partitioning**

We now start considering what type of basic segments may be meaningful for abstraction, that is at what locations a shape is partitioned into separate segments that would be suitable for a parametric description. Figure 4 illustrates the challenge. Most observers would consider the wiggly segments *s1* and *s2* as distinct as compared to the straight segments in the rest of the shape (Fischler and Bolles 1983). However, where exactly the shape is to be partitioned depends on the desired description accuracy: for a loose shape description segment *s1* may constitute a basic segment, but for an accurate shape description, the segment would be partitioned more locally, e.g. it would be further partitioned into smaller segments. Thus, even the process of contour partitioning is an issue of scale selection to some extent.

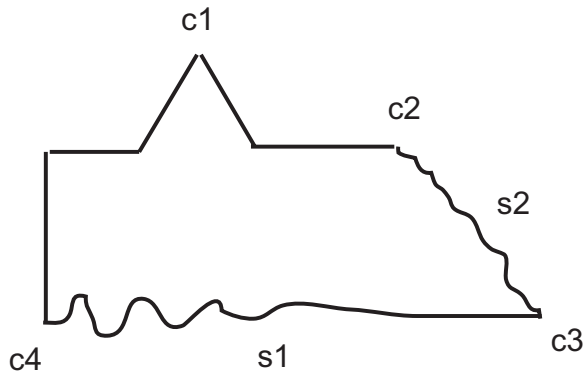


Figure 4: A complex shape illustrating the challenges of contour partitioning and contour representation [figure adapted from (Fischler and Bolles 1983)].

The discrimination between smooth and wiggly segments is again an issue of scale selection. For instance, the contour segment stretching from point c1 to c3 (over point c2) can be considered as wiggly when judged on a more global scale. In fact, that contour segment may constitute a characteristic segment for shape description, as any type of characteristic abstraction facilitates the assignment to its category.

If this shape were part of a complex gray-scale scene – e.g. accidentally emerged due to similar contrasts values for example - , then the issue of partitioning is even more intricate. For instance, if the contours s1 and s2 were part of natural objects - e.g. the silhouette of trees or bushes -, then corner c2 is accidental and were ideally used as a partitioning point. Thus, at the level of shapes and scenes, contour partitioning is also a contextual issue.

Although it seems impossible to define strict partitioning rules - due to this scale and context dependence -, we intuitively think that the local-global space is only suitable for describing elongated or circular contours. The reasoning is that if contour segments lie opposite of each other, then they are more precisely described as two individual segments with a certain structural relation, e.g. by the use of symmetric axes (Blum 1973). A contour is therefore partitioned at high curvature points of *ends* (or U-turns).

Exemplifying this rule on a simple shape, an ellipse is partitioned into its 2 elongated arcs. The shape in figure 4 is partitioned at points c1, c3 and c4 for instance. An end can be easily detected by determining when the arc length  $\omega$  of a selected segment for a given window size exceeds the length of a half circle with diameter  $l$  (the straight line connecting its endpoints). After application of this rule, the remaining partitioned segments are elongated in a global sense. But the rule also partitions smooth arcs whose arc length is larger than half a circle. Such high-circular arcs are preferably extracted before partitioning takes place and can be identified by exploiting the block parameters circularity and edginess ( $\zeta^{\square}$  and  $\varepsilon^{\square}$ , respectively).

[Figure 5]

### Description

To arrive now at a global description of the contour's geometry, the LG space needs to be abstracted such that it expresses the contour's alternating (or 'swinging') behavior. As our method is based on identifying curved segments, the alternating behavior can be captured by determining the fraction of curved segments for a contour. Specifically, a function is created which determine the fraction of (positive) signature values for each window size, forming so the bowness-fraction function,  $\Phi^b(\omega)$ , and the inflexion-fraction function,  $\Phi^r(\omega)$  (see figures 3 to 5, right column, graph 'Fraction'). For a contour consisting of a single *inflexion* (figure 3),  $\Phi^r$  increases with increasing window size - as the contour describes an inflexion at the global level - whereas the inflexion-fraction function  $\Phi^b$  decreases. For an *arc*, the course of the two fraction functions is reversed,  $\Phi^b$  is increasing,  $\Phi^r$  is decreasing (figure 5). The rate of increase and decrease depends on the degree of smoothness (or 'wiggleness'); for example, for a smooth arc  $\Phi^b$  increases rapidly, for a wiggly arc it increases slowly. The location of the increase depends on the degree of circularity for the arc: for a high-circular arc  $\Phi^b$  increases at a more local level, for a low-circular arc  $\Phi^b$  rises at a more global level. For an *alternating* contour (irregular or regular), both fraction functions increase initially and then decrease toward 0 at a global level (figure 6). The maximum of the inflexion-fraction function occurs at a more global level than the maximum of the bowness-fraction function. The locations of the maxima indicate at which level the contour shows its 'strongest' alternating behavior. For a sinusoidal contour of high frequency, the maximal peaks occur at a very local level. These examples illustrated that the course of the fraction functions already express the contour's global geometry. The examples correspond to cardinal values of a continuum of sign changes (occurring on a global level): for an arc there are no such global sign change (value = 0), for an inflexion there is one, and for alternating contours there are two or more.

[Figure 6]

One possibility would be to represent this continuum as a single variable. The difficulty of pursuing this idea is that the variety of contour geometries is rather unlimited and that a contour representation must include other aspects, which are difficult to express in combination with this continuum. Instead, we classify contours into either 'arc' or 'alternating'. The risk of such a classification is that the presence of structural variability can lead to a combinatorial explosion e.g. the same object may be described by different contour types (Draper, Hanson et al. 1996). Instead, we express a contour in a multi-

dimensional space by using the geometric parameters as dimensions. The structural variability then appears as a subspace of this multi-dimensional space.

A contour is classified as an arc ( $a=1$ ), if the bowness-fraction function continuously increases, otherwise the value is 0. This will classify L features also as arcs but those can be distinguished by the edginess value  $\epsilon$ . The degree of curvature (dimension  $b$ ) is defined as the maximal amplitude of the bowness signature for the largest window size. If the segment was not classified as an arc, then it is of type alternating. To characterize this geometry, the window level is selected at which the ratio between the inflexion- and the bowness-fraction functions is closest to the value equal 1 (see vertical bar at window level no. 5 in figure 6). At this window level, the maximal bowness signature value is taken as the curvature value (dimension  $b$ ) and the number of bowness function blocks ( $n_\beta$ ) is used to generate the dimension alternating  $x=\log(n_\beta)$ . Thus, the alternating dimension is scalar whereas the arc dimension is binary.

Another geometrical aspect we describe is the degree of edginess  $e$ , which is taken as the average of all edginess values of all bowness function blocks (of the entire space). An arc contour can have an edginess value larger than 0 if it is wiggly. An alternating contour has a high edginess value if it is a zig-zag line (see figure 8 bottom row). Another aspect is the degree of symmetry  $s$ , which is also taken as the average of all symmetric values. To those 5 geometrical parameters, we add the parameters orientation ( $o$ ) and length ( $l$ ), forming so a 7-dimensional vector  $\mathbf{c}$ :  $\mathbf{c}(o, l, a, x, b, e, s)$ .

### ***Implementation and Evaluation***

The contour description was tested on the COREL collection. The full Corel collection provides 100 image classes, of which 357 belong to a human subordinate category. These were pooled into 112 basic-level categories ((Rasche 2009); basic-level categories as defined by (Rosch, Mervis et al. 1976; Oliva and Torralba 2001). To extract contours, the gray-scale image  $I$  was processed with the Canny algorithm (Canny 1986). A block's symmetry  $v$  is determined by integrating the absolute difference between the first block half and its reversed second block half, which then is normalized. A symmetry value of 0 means complete symmetry (or high regularity), a large value corresponds to high asymmetry (or high irregularity). The fraction functions were implemented by integrating the sign of all function blocks and normalizing by contour length ( $l_c$ ):  $\Phi^\beta(\omega) = [\int_v \text{sgn}(\beta_\omega(v))] / l_c$ . The remaining dimensions are determined without notable issues.

[Figure 7]

A summary of the decomposition output is shown in figure 7. The contour marked no. 1 (silhouette fragment spanning elbow, torso and leg) exemplifies again the challenge of

contour partitioning. The contour was not partitioned and was classified as alternating, and as such it may be very characteristic for this category (see also figure 8 bottom row in (Rasche 2009) for similar contours, that are typical of a person's silhouette). But its elementary straight and curved segments could be locally grouped with other neighboring contours. For instance the straight segment describing the leg of a person's silhouette, forms a parallel grouping with the straight segment of the other side of the leg (no. 1). The LG space offers to identify such elementary segments. But as with detection of high-curvature points, this segment identification is a scale and context-dependent issue and could occur at different local/global levels as it is a priori not clear what the appropriate level of description is. Because this image contains many long (global) contours, we contrived an algorithm, that extracted global segments first but that would still allow for the extraction of smaller (still large) segments. The LG space in figure 3 serves as an example: the bowness block with the largest spatial extension of the LG space is identified, see window no. 6 (block ranging from  $v=1$  to  $v=39$ ); the location of the block's maximal amplitude is taken as the point of highest curvature (indicated by a circle in the contour display [figure 3, upper right]). This maximum block suppresses more local (but not all local) bowness blocks during subsequent extractions (the bowness blocks in windows no. 5 and 4). This identification and suppression procedure is repeated until all large blocks are identified. For the contour in figure 3 there are three curved segments and those are outlined by the horizontal lines in the LG space at a value of ca. 0.4. A minimum block size was set and that is the reason why only one more local curved segment was detected. An analogous extraction algorithm is applied to select straight segments, which are indicated as squares. Returning to figure 7, closely spaced or overlapping circles - such as the curved segment of the torso in contour no. 1 - indicate that global and local segments were detected.

The effect of parameter variations is demonstrated in figure 8 by a similarity search for contours with preferred parameters. The top row contains contours, whose preferred geometry was an arc with low edginess and high symmetry value. From left to right the bendness value ( $b$ ) was systematically increased from 0.2 to 1.0. For high curvatures, the degree of circularity appears non-linear due to the aliasing problem (in this case arc length differences). The 2<sup>nd</sup> row contains searches for alternating contours whose preferred bendness value increases again from left to right; the contour's 'oscillating' amplitude increases correspondingly. The bottom row contains searches for alternating contours with increasing edginess value ( $e$ ).

The contour in image no. 7789 (lower left plot in figure 8) uncovers again the difficulty of contour description. While this contour was determined as wiggly it may in this specific case be better to express it as a precise sequence of straight and curved segments.

[Figure 8]

The contour description can represent segments that are typical for categories (figure 9). Those contours were selected from pairs of images of the same category by matching the contours of one image against those of the other image. Only similar contours were kept using a simple thresholding mechanism (similar to a method used in (Rasche 2009)). This was carried out at different fine/coarse scales ( $\sigma = 1, 3$  and  $5$ ; left, middle and right column in figure 9). For this selection we have also used appearance parameters: 2 pairs of parameters describing the mean and standard deviation of the contrast and fuzziness values along the contour ( $c_m, c_s, f_m, f_s$ ; 11-dimensional vector). The fuzziness values are obtained from a simple blob filter that was convolved with the image  $I$ .

[Figure 9]

For an evaluation of other image collections, such as the Caltech 101 collection (Li, Fergus et al. 2006), or the Natural&Urban collection (Oliva and Torralba 2001), see our technical study (Rasche 2009). As a distance measure the radial-basis function was employed. Using the Euclidean distance function did not change search results as in figure 8 and 9 significantly. A number of different, exact definitions for some of the dimensions were tested. All these variations did not alter overall performance significantly.

## **Discussion**

The local/global space for contours is not meant to be a replacement for the fine/coarse scale (scale space). A coarse image is necessary for instance for generating continuous contour segments for natural contours, but it is the LG space for individual contours which allows an exhaustive geometric description. Thus, for visual recognition of gray-scale images both spaces are necessary.

The LG space enables to find high-curvature points, curved segments and straight segments. This selection is however scale- and context-dependent issue (figure 3), so are the processes of contour partitioning and contour abstraction (figure 4). In this study, only one context-free (strict) partitioning rule is applied, the partitioning of ‘ends’. A shape (or any structure) can be easily partitioned by a human observer, once the semantic content (category) of the structure was known. But this information is obtained so quickly (e.g. (Potter 1975; Thorpe, Fize et al. 1996; Schendan, Ganis et al. 1998)), that it raises the question to what degree partitioning takes place before this fast categorization has occurred. We see two possible solutions. 1) A contextual analysis takes place that determines whether further partitioning (beyond splitting at U turns) is

meaningful. 2) Multiple, overlapping descriptions are extracted: for instance contour no 1 in figure 7 is left unpartitioned, because it is potentially very category-specific; in addition, the identified elementary segments are extracted as well, as those are useful for grouping.

We have concentrated on three basic geometries, straight, arc and wiggly (for contour description). But other basic descriptions may be possible, such as an inflexion, a contour that occurs in many animal silhouettes (outlining the animal's back and neck). One can therefore assume that there exist mechanisms selecting this type of geometry and possibly other geometries. Such descriptions can be easily derived from the LG space.

The set of geometric contour parameters derived from the LG space is accurate but likely not precise enough for subordinate categorization or identification. For face identification for instance, the subtle contour geometry is decisive and must therefore be expressed more distinctively. Such higher distinctness can be achieved by parameterizing function blocks in greater detail as we suggested in figure 1c, d and e. Psychophysical and neurophysiological studies have shown that such high-precision parameterization can take place (e.g. Riggs, 1973; Whitaker et al, 1998).

The principle of the LG space may also be suitable to express other types of neural representation. For instance, the tactile representation of an exploratory movement describes a time-space trajectory (e.g. (Drewing and Ernst 2006)), that can be regarded as a two-dimensional contour. The parametric description of such trajectories may require a more exact representation than was used here, but as hinted above, the LG space contains a large repertoire of geometrical aspects from which a higher degree of precision can be extracted.

What other psychophysical evidence exist for this decomposition? We think the strongest hint comes from the search studies on *parallel* pop-out, e.g. by Treisman and Gormican (Treisman and Gormican 1988). Such studies show that humans rapidly detect small deviation in structure such as the orientation of short contours, their length, their curvature (see their figures 2, 5, 6 and 11). Modeling studies mimicking visual search explain these variances by template matching essentially (Itti and Koch 2001; Li 2002), thereby following the idea of feature detection (Treisman 1988). In contrast, the present approach can detect these variances by determining the differences for individual dimensions (see for instance figure 8 top row for curvature differences). One criticism of these pop-out effects is that many pop-out experiments can be contrived: For instance, a single, wiggly segment likely pops out amongst smooth segments. But the decomposition presented here could possibly explain all such contour pop-outs.

Those pop-out effects are generally interpreted as supporting the traditional viewpoint of recognition evolvment, namely that of a gradual local-to-global integration along a hierarchy spanning several visual areas (Hubel and Wiesel 1968; Barlow 1972; Essen, Felleman et al. 1990). But a newer viewpoint is that some form of global integration

already takes place in early visual cortical areas using for instance horizontal connections amongst cells of the same neocortical layer, thus arguing rather for a global-to-local recognition evolution, e.g. (Kovacs 1996; Li 1998; Pettet, McKee et al. 1998; Hess and Field 1999; Rasche and Koch 2002). What then could possibly be a neurally plausible computational substrate for the presented decomposition? The geometrical aspects of a contour could be read out from a histogram of the contour's local orientations: the distribution's width corresponds to the degree of curvature or circularity and the location of the maximum to the contour's orientation. The use of such orientation histograms for structural description has already been suggested (Stevens 1978; Renninger, Verghese et al. 2007). Pursuing this principle, a next step would be to include directional information to discriminate between bow and inflexion. Neurophysiological studies have found neurons coding for curvature, but their integration mechanisms have been interpreted according to the traditional viewpoint of a local-to-global recognition evolution (Dobbins et al, 1987; Brincat and Connor, 2004).

### ***Acknowledgements***

CR is supported by the Gaze-based Communication Project (contract no. IST-C-033816, European Commission within the Information Society Technologies).

### ***References***

Attneave, F. (1954). "Some informational aspects of visual perception." Psychological Review **61**(3): 183-193.

Barlow, H. B. (1972). "Single units and sensation: a neuron doctrine for perceptual psychology?" Perception. **1**(4): 371-94.

Blum, H. (1973). "Biological Shape And Visual Science .1." Journal Of Theoretical Biology **38**(2): 205--287.

Canny, J. (1986). "A COMPUTATIONAL APPROACH TO EDGE-DETECTION." IEEE Transactions on Pattern Analysis and Machine Intelligence **8**(6): 679--698.

Coen-Cagli, R., P. Coraggio, et al. (2009). "Visumotor characterization of eye movements in a drawing task." Vision Research **49**: 810-818.

Draper, B. A., A. R. Hanson, et al. (1996). "Knowledge-directed vision: Control, learning, and integration." Proceedings of the IEEE **84**(11): 1625--1637.

Drewing, K. and M. O. Ernst (2006). "Integration of force and position cues for shape perception through active touch." BRAIN RESEARCH **1078**: 92-100.

Essen, D. C. V., D. J. Felleman, et al. (1990). "Modular and hierarchical organization of extrastriate visual cortex in the macaque monkey." Cold Spring Harb Symp Quant Biol **55**: 679-96.

Feldman, J. (2001). "Bayesian contour integration." Perception & Psychophysics **63**(7): 1171--1182.

Fischler, M. A. and R. C. Bolles (1983). Perceptual organization and the curve partitioning problem. Proceedings of the Tenth International Joint Conference on Artificial Intelligence, Volume 2.

Hansen, T. and H. Neumann (2004). "Neural mechanisms for the robust representation of junctions." Neural Computation **16**(5): 1013--1037.

Hess, R. and D. Field (1999). "Integration of contours: new insights." Trends In Cognitive Sciences **3**(12): 480--486.

Hubel, D. H. and T. N. Wiesel (1968). "Receptive fields and functional architecture of monkey striate cortex." The Journal of physiology **195**(1): 215-43.

Itti, L. and C. Koch (2001). "Computational modelling of visual attention." Nature Reviews Neuroscience **2**(3): 194--203.

Kovacs, I. (1996). "Gestalten of today: Early processing of visual contours and surfaces." Behavioural Brain Research **82**(1): 1--11.

Li, F. F., R. Fergus, et al. (2006). "One-shot learning of object categories." IEEE TRANSACTIONS ON PATTERN ANALYSIS AND MACHINE INTELLIGENCE **28**(4): 594-611.

Li, Z. P. (1998). "A neural model of contour integration in the primary visual cortex." Neural Computation **10**(4): 903--940.

Li, Z. P. (2002). "A saliency map in primary visual cortex." Trends In Cognitive Sciences **6**(1): 9--16.

Oliva, A. and A. Torralba (2001). "Modeling the shape of the scene: A holistic representation of the spatial envelope." Int. J. Comput. Vis. **42**(3): 145-175.

Pettet, M. W., S. P. McKee, et al. (1998). "Constraints on long range interactions mediating contour detection." Vision research. **38**(6): 865-79.

Potter, M. C. (1975). "Meaning in visual search." Science **187**(4180): 965-6.

- Rasche, C. (2009). "An Approach to the Parameterization of Structure for Fast Categorization." INTERNATIONAL JOURNAL OF COMPUTER VISION **accepted**.
- Rasche, C. and K. Gegenfurtner (2010). "Visual Orienting in Dynamic Broadband (1/f) Noise Sequences." Attention, Perception and Psychophysics **accepted**.
- Rasche, C. and C. Koch (2002). "Recognizing the gist of a visual scene: possible perceptual and neural mechanisms." NEUROCOMPUTING **44**: 979--984.
- Renninger, L. W., P. Verghese, et al. (2007). "Where to look next? Eye movements reduce local uncertainty." Journal of Vision **7**: 1-17.
- Riesenhuber, M. and T. Poggio (1999). "Hierarchical models of object recognition in cortex." Nature Neuroscience **2**(11): 1019--1025.
- Rosch, E., C. B. Mervis, et al. (1976). "Basic objects in natural categories." Cognitive Psychology **8**: 382-439.
- Schendan, H. E., G. Ganis, et al. (1998). "Neurophysiological evidence for visual perceptual categorization of words and faces within 150 ms." Psychophysiology **35**(3): 240-51.
- Stevens, K. A. (1978). "Computation of locally parallel structure." Biological Cybernetics **29**: 19-28.
- Tatler, B. W., R. J. Baddeley, et al. (2005). "Visual correlates of fixation selection: effects of scale and time." Vision Research **45**(5): 643--659.
- Thorpe, S., D. Fize, et al. (1996). "Speed of processing in the human visual system." Nature **381**: 520-522.
- Treisman, A. (1988). "Features and objects: the fourteenth Bartlett memorial lecture." Q J Exp Psychol [A] **40**(2): 201-37.
- Treisman, A. and S. Gormican (1988). "Feature analysis in early vision: evidence from search asymmetries." Psychol Rev **95**(1): 15-48.
- VanRullen, R. and S. J. Thorpe (2002). "Surfing a spike wave down the ventral stream." Vision Research **42**(23): 2593--2615.

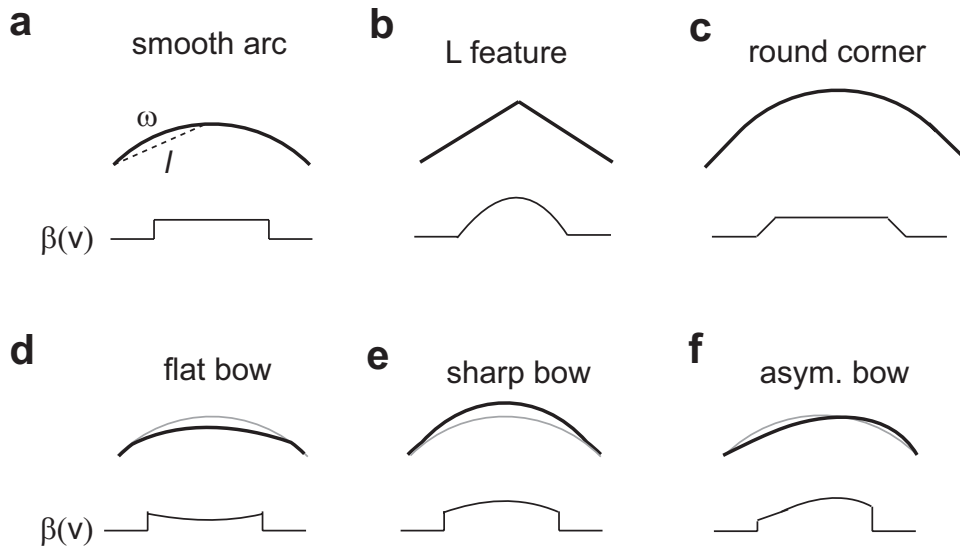


Figure 1: Signature of basic contour geometries for a given window size. A chord (stick) of fixed length  $\omega$  is iterated through the contour and the amplitude (maximal distance) between the straight line  $l$  and the subsegment determined. If the subsegment lies primarily on one side of the straight line, then its amplitude is assigned to the 'bowness' signature  $\beta(v)$ . **a-f.** Bowness signature for various geometries (gray=perfect bow or arc).

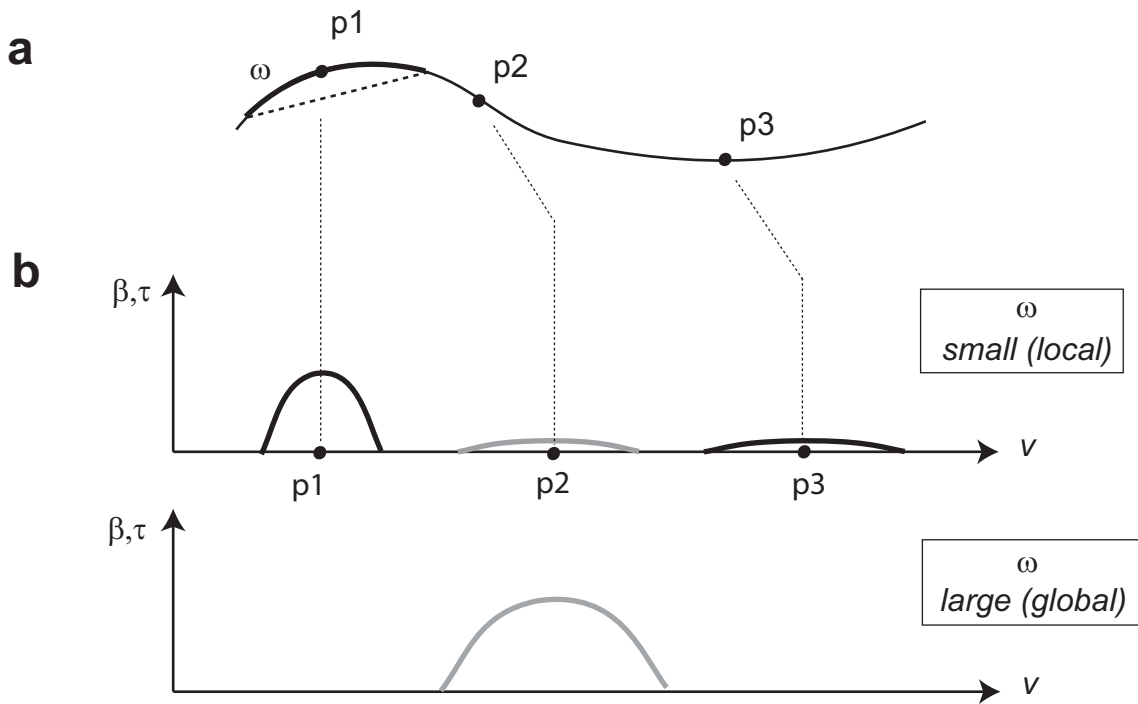


Figure 2: Schematic of the local/global space for a contour (inflexion). **a.** A contour with two points of high curvature (p1, p3) and one change of sign (p2). **b.** LG space illustrated for two window sizes, small (local) and large (global): each graph plots the bowness and inflexion signature ( $\beta$ ,  $\tau$ , black and gray respectively;  $v$ : arc length of the contour).

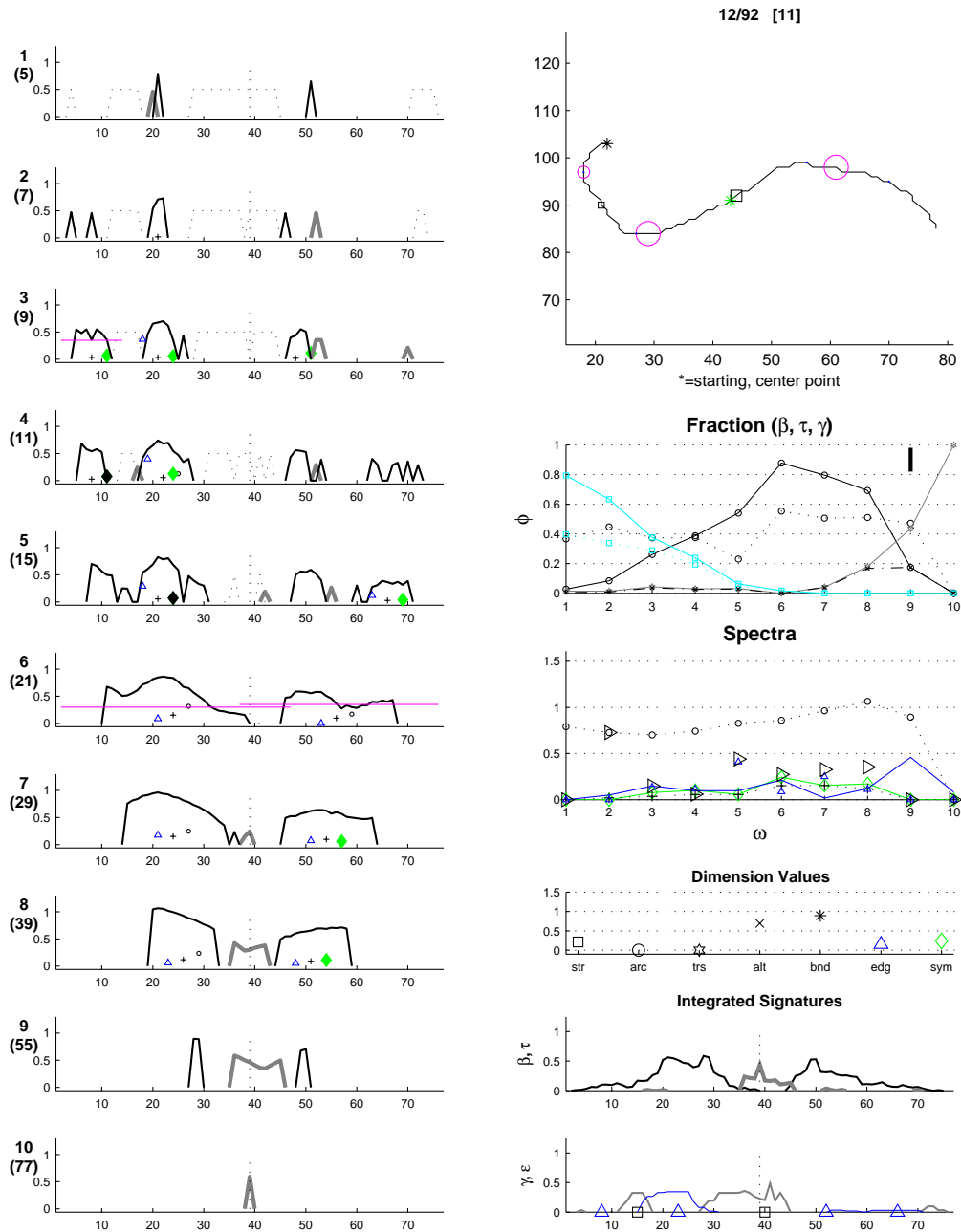


Figure 3: Local/global space for an inflexion contour. **Upper right**: sample contour with starting and center point marked as asterisk. **Left column**: LG space: signatures  $\beta$  (thick black),  $\tau$  (grey),  $\gamma$  (stippled). Window number and size (in pixels) given on left of each signature graph. Function block characteristics (determined for large ones only): triangle marker =  $\varepsilon^{\square}$  (edginess); diamond marker =  $\nu^{\square}$  (symmetry); plus sign marker =  $\zeta^{\square}$  (circularity). **Center right**: **Fraction**: fraction  $\Phi$  of bowness- and inflexion-function blocks per window size. **Spectra**: Green diamond: maximum of symmetry value; black circle: maximum  $\beta$  amplitude; plus sign: maximum of  $\zeta$ . **Dimension Values**: str=straightness (not used), arc, alt=alternation, trs=transition (not used), bnd=curvature, edg=edginess, sym=symmetry. **Integrated Signatures**: top graph: bowness (black), inflexion (gray); bottom graph: edginess (triangles) and straightness (squares).

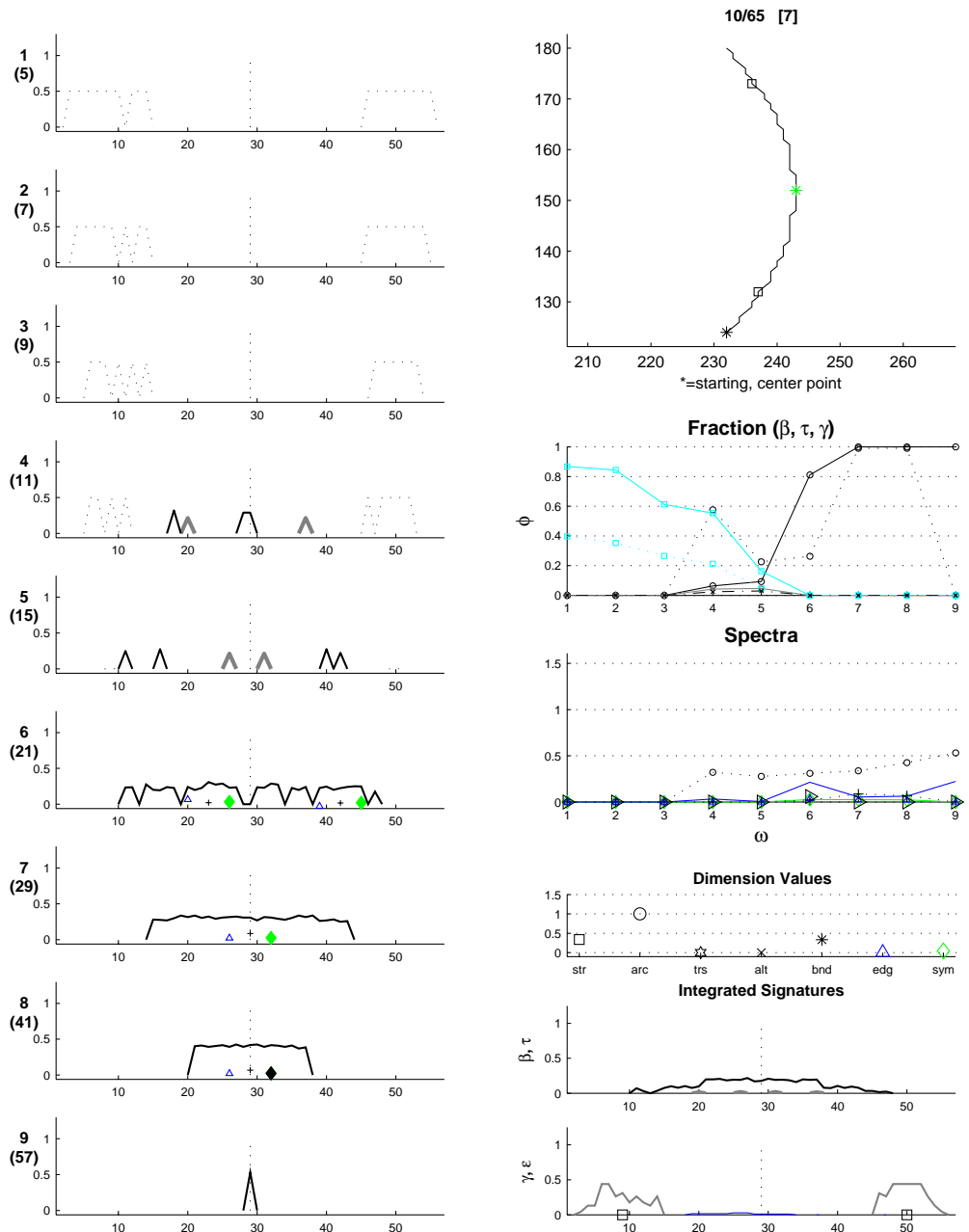


Figure 5: Local/global space for an arc contour. Note that the bowness-fraction function continuously increases up to the value of 1, the inflexion-fraction function shows a small elevation at window levels 4 and 5 due to noisiness.

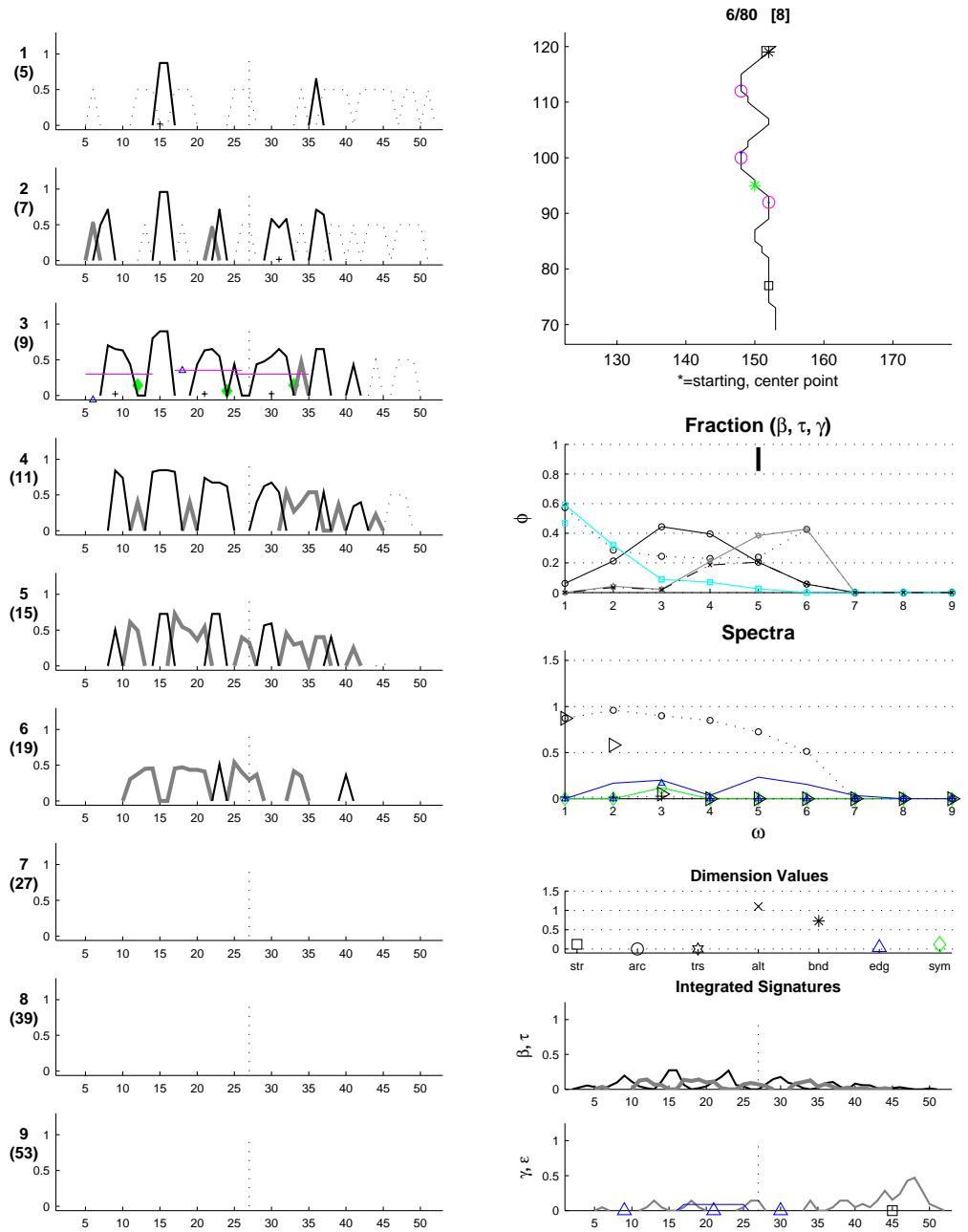


Figure 6: Local/global space for a wiggly contour (similar to segment s1 in figure 4). Note that both fraction functions show a bump at a lower window level with the one for inflexion appearing at a slightly more global level. The vertical bar at window level 5 (top) denotes the window level at which the 'oscillating' nature of the contour is largest.

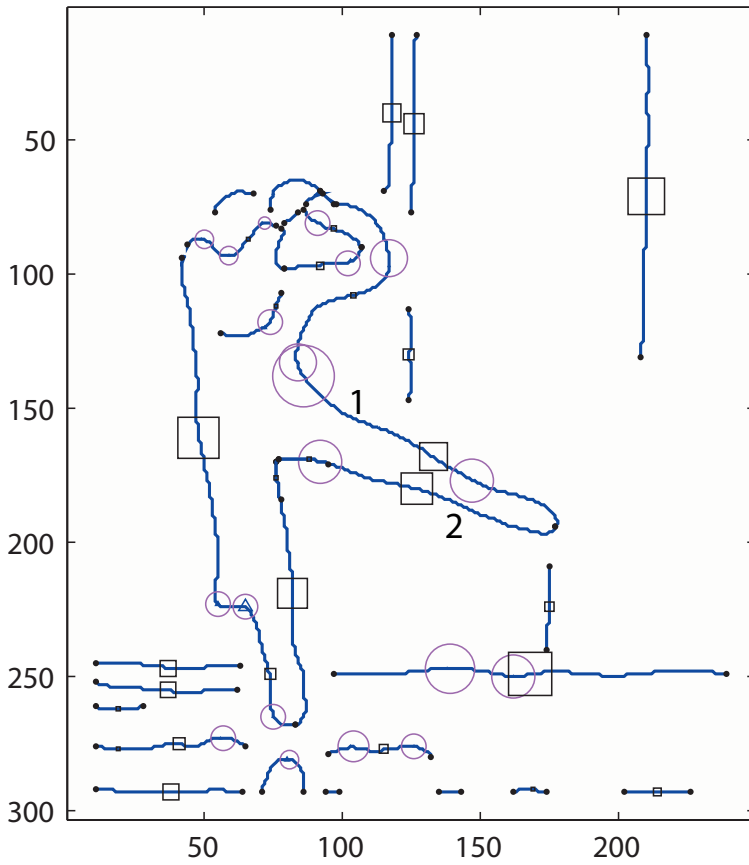


Figure 7: Decomposition output for an image (silhouette of a ballerina). Contour endpoints are marked as small black circles; squares and circles denote straight and curved segments respectively (their size reflects segment length – not curvature). Overlapping circles result from the global-to-local identification of elementary segments.

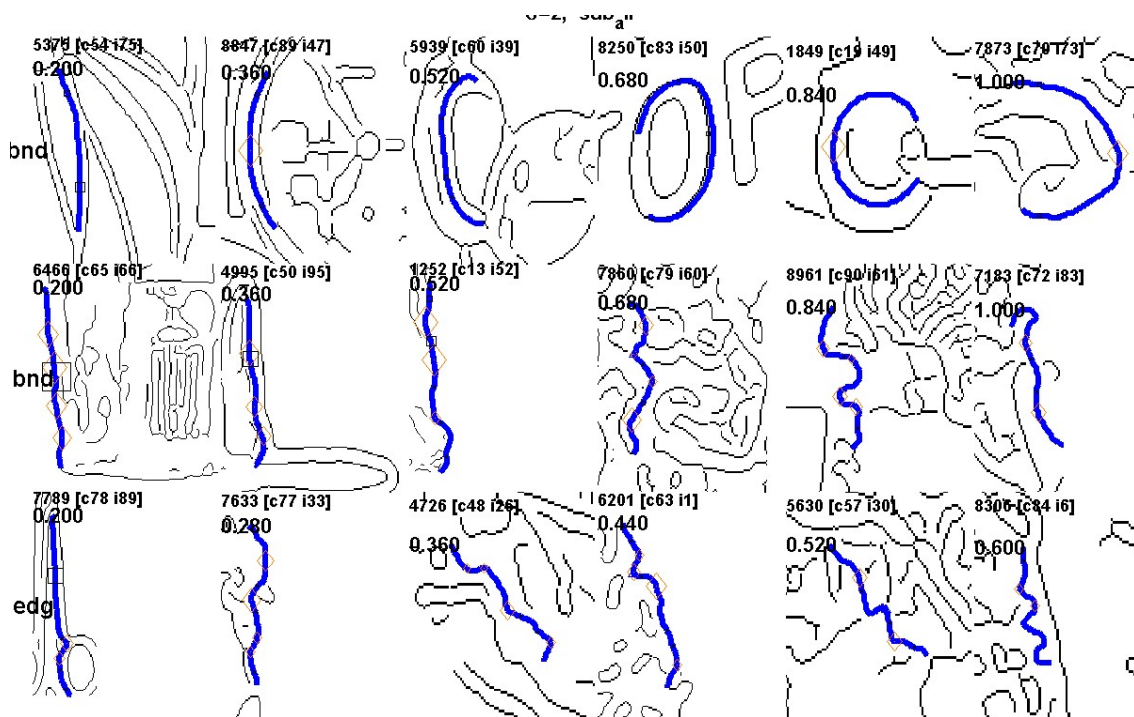


Figure 8: Examples of parameter changes. In the top row, arc-classified contours with increasing curvature values are selected ( $b=0.2\dots1.0$ ). The center row contains alternating contours with increasing curvature ( $b=0.2\dots1.0$ ). The bottom row contains alternating contours with increasing edginess ( $e=0.2\dots0.6$ ).

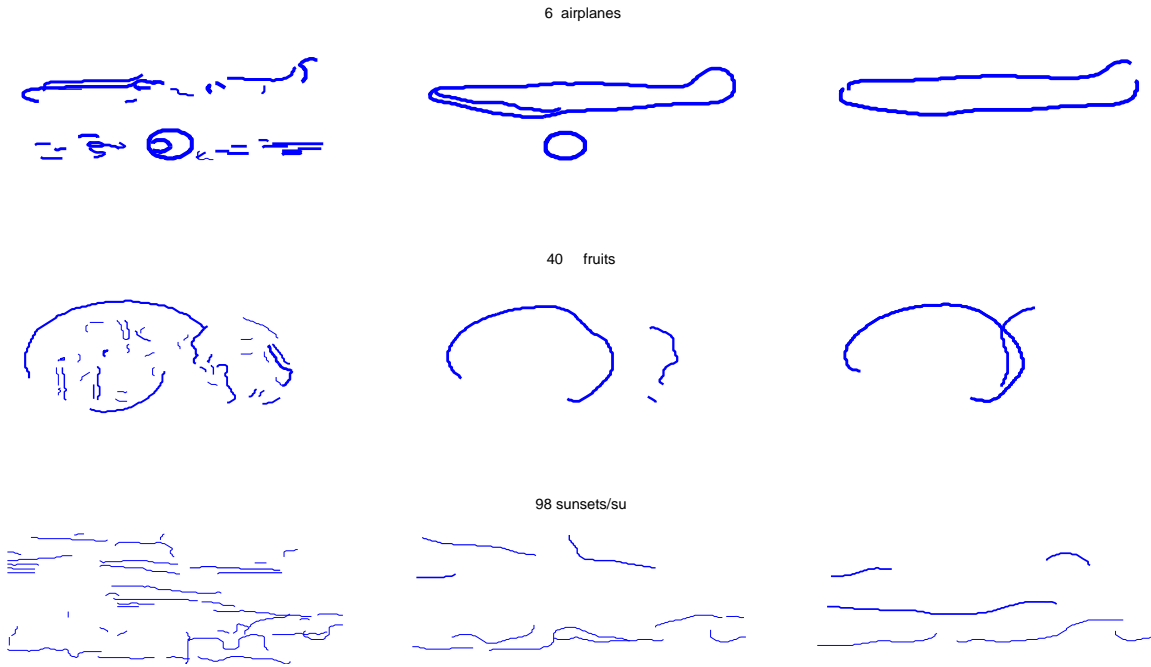


Figure 9: Category-specific contours for 3 basic-level categories of the COREL collection (airplanes [no. 6], fruits [no. 40], sunsets/rises [no. 98]) for fine/coarse scale  $\sigma=1, 3$  and  $5$  (left, middle, right). The contour thickness corresponds to the average contrast value ( $C_m$ ).